AGU PUBLICATIONS

JGR

Journal of Geophysical Research: Solid Earth

RESEARCH ARTICLE
10.1002/2013JB010900

Key Points:
- Band-limited topographic mass model generates a full-spectrum gravity field
- The pth power of topography expanded to n contributes to degree p × n to potential
- Spatial and spectral gravity forward modeling techniques agree at 10–5 level

Correspondence to:
C. Hirt,
c.hirt@curtin.edu.au

Citation:
Hirt, C., and M. Kuhn (2014), Band-limited topographic mass distribution generates full-spectrum gravity field: Gravity forward modeling in the spectral and spatial domains revisited, *J. Geophys. Res. Solid Earth*, *119*, 3646–3661, doi:10.1002/2013JB010900.

Received 10 DEC 2013
Accepted 13 MAR 2014
Accepted article online 20 MAR 2014
Published online 11 APR 2014

Band-limited topographic mass distribution generates full-spectrum gravity field: Gravity forward modeling in the spectral and spatial domains revisited

Christian Hirt[1,2] and Michael Kuhn[1]

[1]Western Australian Centre for Geodesy and Institute for Geoscience Research, Curtin University, Perth, Western Australia, Australia, [2]Now at Institute for Astronomical and Physical Geodesy and Institute for Advanced Study, Technische Universität München, Garching, Germany

Abstract Most studies on gravity forward modeling in the spectral domain truncate the gravitational potential spectra at a resolution commensurate with the input topographic mass model. This implicitly assumes spectral consistency between topography and implied topographic potential. Here we demonstrate that a band-limited topographic mass distribution generates gravity signals with spectral energy at spatial scales far beyond the input topography's resolution. The spectral energy at scales shorter than the resolution of the input topography is associated with the contributions made by higher-order integer powers of the topography to the topographic potential. The *p*th integer power of a topography expanded to spherical harmonic degree n is found to make contributions to the topographic potential up to harmonic degree *p* times *n*. New numerical comparisons between Newton's integral evaluated in the spatial and spectral domain show that this previously little addressed truncation effect reaches amplitudes of several mGal for topography-implied gravity signals. Modeling the short-scale gravity signal in the spectral domain improves the agreement between spatial and spectral domain techniques to the μGal level, or below 10^{-5} in terms of relative errors. Our findings have important implications for the use of gravity forward modeling in geophysics and geodesy: The topographic potential in spherical harmonics must be calculated to a much higher harmonic degree than resolved by the input topography if consistency between topography and implied potential is sought. With the improved understanding of the spectral modeling technique in this paper, theories, and computer implementations for both techniques can now be significantly better mutually validated.

1. Introduction

Gravity forward modeling denotes the computation of the gravitational signal (e.g., in terms of gravitational potential, gravity disturbances, or gravity gradients) induced by a mass-density distribution, as given, e.g., through topographic mass models. Techniques for gravity forward modeling are routinely applied in potential field geophysics, e.g., to aid the interpretation of observed gravity [*Jacoby and Smilde*, 2009] and in physical geodesy, e.g., in the context of geoid modeling [*Tziavos and Sideris*, 2013]. Common to all gravity forward modeling techniques is the evaluation of the well-known Newton's integral, which can be done both in the spatial domain and spectral domain [*Kuhn and Seitz*, 2005; *Wild-Pfeiffer and Heck*, 2007].

1. Spatial domain forward modeling [e.g., *Forsberg*, 1984; *Nagy et al.*, 2000; *Kuhn et al.*, 2009; *Tsoulis et al.*, 2009; *Hirt et al.*, 2010; *Grombein et al.*, 2013; *D'Urso*, 2014] directly evaluates Newton's integral. This is commonly done by decomposing the topographic mass model into elementary bodies (e.g., prisms, tesseroids, and polyhedra) along with numerical/analytical integration to obtain the gravitational potential implied by the masses. This technique is also known as Newtonian integration.
2. Spectral domain forward modeling [e.g., *Sünkel*, 1985; *Rummel et al.*, 1988; *Tenzer*, 2005; *Wieczorek*, 2007; *Novák*, 2010; *Hirt and Kuhn*, 2012] evaluates Newton's integral through transformation into the spectral domain. This commonly utilizes spherical harmonic series expansions for conversion of spherical harmonic topography models to the implied gravitational potential. Formulated as a three-step procedure, in spectral forward modeling (i) the topographic surface (i.e., the topographic heights sampled on a geographical grid)

and its integer powers are expanded into spherical harmonic series. The resulting coefficients are (ii) directly used to yield the topographic potential in spherical harmonics (as a series expansion of the integer powers of the topography), and (iii) gravity effects are obtained from the topographic potential coefficients in the spatial domain through spherical harmonic synthesis.

Many previous studies concerned with spectral domain forward modeling use a spherical harmonic topography model to some fixed spectral resolution (as specified through the maximum harmonic degree of the series expansion, e.g., 360) for the calculation of implied gravitational potential with identical resolution. As such, spectral consistency (i.e., identical spectral bandwidths) of the topography and generated gravitational potential is implicitly assumed. Examples of such works are *Sünkel* [1985], *Rummel et al*. [1988], *Rapp* [1989], *Rapp and Pavlis* [1990], *Pavlis and Rapp* [1990], *Tsoulis* [2001], *Kuhn and Featherstone* [2003], *Wild-Pfeiffer and Heck* [2007], *Wieczorek* [2007], *Makhloof* [2007], *Novák* [2010], *Balmino et al*. [2012], *Hirt et al*. [2012], *Hirt and Kuhn* [2012], *Tenzer et al*. [2012], *Bagherbandi and Sjöberg* [2012], *Novák and Tenzer* [2013], and *Gruber et al*. [2013], among others. However, as will be shown in this paper, this mostly unwritten assumption does not hold [see also *Heck and Seitz*, 1991; *Papp and Wang*, 1996].

As the main topic of the present study we demonstrate that a band-limited spherical harmonic topography generates (in good approximation) a full-banded gravitational potential. We show that the generated gravitational signal features additional high-frequency spectral energy beyond and far beyond the initial band limitation of the input (source) topography. This effect, which causes "spectral inconsistency" between topography and gravitational signal, is fairly straightforward to model (section 2), but mostly neglected in the literature. We will show this effect to be responsible for spurious discrepancies in numerical comparisons among gravitational signals from spectral and space domain techniques (section 3).

In previous studies concerned with comparisons among gravitational effects from the two techniques, notable discrepancies were encountered or reported. In terms of *relative errors* (defined here as the ratio between the maximum discrepancy between spatial and spectral forward modeling and the maximum gravitational signal over some test area) *Kuhn and Seitz* [2005] found relative errors at the level of ~3% for the gravitational potential, for expansions to harmonic degree 1440; *Wild-Pfeiffer and Heck* [2007] yielded relative errors of ~4.5% for gravity gradients over a global test area (maximum signals of ~6.7 E (1 E = 1 eötvös = 10^{-9} s^{-2}) versus a maximum discrepancy of ~0.3 E); *Wang et al*. [2010] encountered relative errors at the level of ~10% or up to ~60 mGal(1 mGal = 10^{-5} m s^{-2}) discrepancies for gravity disturbances over various mountainous test areas (e.g., Himalayas, Rocky Mountains, and Andes) for expansions to harmonic degree 2700; *Balmino et al*. [2012] published discrepancies at the level of ~10% (or up to ~48 mGal) for gravity disturbances over their test area "Marocco"; and *Novák and Tenzer* [2013] found relative errors of ~0.8% for gravity gradients at satellite altitude over a regional test profile crossing the Andes (maximum discrepancy of 0.5×10^{-2} E versus signal of 5.8 E); please also see discussion in section 4. The five aforementioned studies have in common that they do not investigate the spectral inconsistency between topography and implied gravity as a key candidate for the differences encountered. While the spatial domain technique (Newtonian integration) implicitly takes into account the additional high-frequency spectral constituents beyond the bandwidth of the input topography, explicit consideration is required in the spectral domain for improved mutual consistency of gravity effects from the two forward modeling techniques.

From our literature review, the spectral inconsistency among topography and gravity is only little discussed in the context of gravity forward modeling, though the mechanisms affecting the spectral characteristics are by no means unknown. *Papp and Wang* [1996] modeled the gravitational potential in spherical harmonics and noticed truncation effects in comparisons with Newtonian integration. They made the important statement that "[…] the spectral characteristics of the spherical harmonics in forward local gravity modeling are different from that of the results obtained from rectangular prism integration." [*Papp and Wang*, 1996, p. 63]. *Heck and Seitz* [1991] investigated nonlinear effects in the geodetic boundary value problem, showing that the multiplication of two series expansions to represent second-order effects increases the maximum harmonic degree by a factor of 2. In the context of the frequently used geodetic reference system (GRS80) [*Moritz* [2000]], another analogy is found (S. Claessens, personal communication, 2013). A rotating mass ellipsoid (as "example" for a most simple spherical harmonic topography) generates a gravitational field with notable spectral energy at even multiples of degree 2.

The first and main aim of the present study is the introduction of a novel contribution scheme for spectral domain forward modeling that relies on spherical harmonic topographic mass models of some given resolution as input data. Our scheme provides the spectral constituents of the implied gravity signal at all spatial scales—to and beyond the input topography's resolution. As second aim of the study, we use the contribution scheme in new comparisons between spectral and spatial forward modeling techniques to demonstrate that high-frequency gravity signals (beyond the input topography's resolution) are naturally "delivered" by space domain techniques, while the spectral technique requires explicit modeling. Our new contribution scheme is suitable to do this. As further aims, we demonstrate the practical relevance of the higher-order integer power contributions of the topography to the implied potential, the importance of the computation point height in both techniques, and the convergence of series expansions used for field continuation in the spectral domain.

The paper is organized as follows. Section 2 sets the mathematical framework for spatial and spectral domain forward modeling, exemplified here for gravity disturbances as radial derivatives of the gravitational potential. Section 3 then presents a numerical case study which (i) analyzes the spectra of the topography-implied gravitational potential and (ii) compares gravity from spatial and spectral domain forward modeling. The case study demonstrates that explicit modeling of the high-frequency spectrum in the spectral domain significantly improves the agreement with spatial forward modeling. Section 4 discusses the results, also in the context of the literature, and section 5 draws conclusions for some present and future gravity forward modeling applications.

2. Theory

We start by introducing H_{nm} as a shorthand for the fully normalized spherical harmonic coefficients (SHC) $\left(\overline{\mathrm{HC}}, \overline{\mathrm{HS}}\right)_{nm}$ of a topography model, whereby n denotes the harmonic degree and m the harmonic order. The coefficients H_{nm} are expanded into the spherical harmonic series

$$H(\varphi,\lambda) = \sum_{n=0}^{n_{\max}} \sum_{m=0}^{n} \left(\overline{\mathrm{HC}}_{nm} \cos m\lambda + \overline{\mathrm{HS}}_{nm} \sin m\lambda\right) \overline{P}_{nm}(\sin\varphi) \tag{1}$$

to maximum degree $n_{\max}$ in order to describe the topographic height $H(\varphi,\lambda)$ at geocentric latitude φ and longitude λ. The term $\overline{P}_{nm}(\sin\varphi)$ denotes the fully normalized associated Legendre function of degree n and order m. Topographic heights H are laterally variable and provide the height of the topographic surface with respect to some height reference surface, e.g., mean sea level. The harmonic coefficients H_{nm} are assumed to be readily available from a spherical harmonic analysis of some global topography model (cf. section 3).

The spherical harmonic topography model expanded to maximum degree $n_{\max}$ is used as input (i.e., source model that generates the topographic gravity field) both for the spatial domain (section 2.1) and spectral domain forward modeling (section 2.2) along with some constant mass-density value ρ (e.g., of standard rock). This is done in order to use identical topographic mass models as "source of the gravity field" in both techniques. We acknowledge that laterally varying mass-density values could be used as a refinement [e.g., *Kuhn and Featherstone*, 2003; *Eshagh*, 2009], but this is not necessary for the topic of our study.

For reasons of simplification, we consistently use the spherical approximation for forward modeling with both techniques. In the spherical approximation, the topographic height H is "mapped" onto the surface of a reference sphere with some constant radius R [see, e.g., *Balmino et al*., 2012]. The spherical approximation is chosen here over the more advanced ellipsoidal approximation [*Claessens and Hirt*, 2013; *Wang and Yang*, 2013] which uses a reference ellipsoid instead of a reference sphere. The spherical approximation level chosen is completely suitable to compare the spectral characteristics of the topography with the implied topographic potential. The spherical approximation is also used for reasons of consistency with the vast majority of previous works on forward modeling (see references in section 1).

2.1. Spatial Domain Forward Modeling

Spatial domain forward modeling of the global topographic masses is based on *discretized* Newtonian integration following the concepts applied in, e.g., *Kuhn* [2000, 2003] and *Kuhn et al*. [2009]. In this approach the mass distribution considered is discretized by a set of regularly shaped mass elements (e.g., point mass, prism, or tesseroid), and the gravitational signal is obtained through superposition of the individual effects

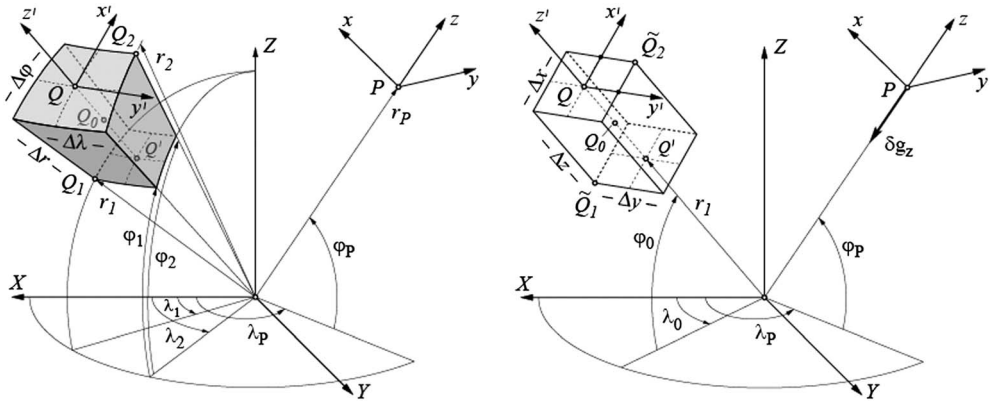

Figure 1. Geometry of a (left) tesseroid replaced by a rectangular prism with first-order mass equivalence and (right) identical vertical extension. Note, while the intersection points Q and Q' of the center line with the tesseroid's top and bottom surfaces are identical with that of the prism, the corner points are not (e.g., $Q_1 \neq \widetilde{Q}_1$ and $Q_2 \neq \widetilde{Q}_2$).

from each mass element. This principle is exemplified by equation (2) through Newton's integral for the gravitational potential δV generated by the mass distribution M replaced by the sum over the gravitational potentials δV_n generated by N_{elem} mass elements m_n ($n = 1, \ldots, N_{\text{elem}}$).

$$\delta V = G \iiint_M \frac{\mathrm{d}m}{l} \approx \sum_{n=1}^{N_{\text{elem}}} G \iiint_{m_n} \frac{\mathrm{d}m_n}{l_n} = \sum_{n=1}^{N_{\text{elem}}} \delta V_n \tag{2}$$

In equation (2), G is the universal gravitational constant, and $\mathrm{d}m$ and $\mathrm{d}m_n$ denote infinitesimally small mass elements describing M and m_n, respectively. The Euclidian distances l and l_n are defined between the computation point P and the running integration points within M and m_n, respectively. We calculate the gravitational attraction δg_z (radial derivative of the potential, also known as gravity disturbance) along the vertical at P (i.e., in opposite direction to the surface normal on a reference sphere) via

$$\delta \vec{g} = \left(\delta g_x, \delta g_y, \delta g_z\right)^T = \mathrm{grad}(\delta V) \approx \sum_{n=1}^{N} \mathrm{grad}(\delta V_n) \tag{3}$$

where grad denotes the gradient and δg_x, δg_y, and δg_z are the vector components of $\delta \vec{g}$ given with respect to a topocentric coordinate system x, y, and z at P (cf. Figure 1). The coordinate axes of the topocentric coordinate system are orientated so that the x axis points toward geodetic north, the y axis toward geodetic east, and the z axis toward the zenith (or radial direction).

The approximation errors introduced by equations (2) and (3) depend on how well the elements m_n approximate the original mass distribution M. The use of rectangular prisms is approximate because the vertical faces of adjoining prisms are not parallel (they intersect or exhibit wedge-like gaps). An upper limit of the magnitude of this effect on the order of 2 μGal ($= 2 \times 10^{-8}\,\mathrm{m\,s^{-2}}$) in this study is obtained from the numerical comparisons between the space and spectral domain techniques (section 3.4). In future application of the space domain technique, polyhedra [e.g., *Benedek*, 2004; *D'Urso*, 2014] can be a viable alternative to prisms because they avoid the prism approximation. In order to reduce approximation errors caused by mass elements located in the vicinity of the computation point, we divide the gravitational attraction according to

$$\delta \vec{g} = \delta \vec{g}^{\,\mathrm{SH}} + \delta \vec{g}^{\,\mathrm{RM}} \tag{4}$$

where $\delta \vec{g}^{\,\mathrm{SH}}$ is the gravitational attraction of a shell (or more generally a layer) of constant thickness and $\delta \vec{g}^{\,\mathrm{RM}}$ is the gravitational attraction of all masses residual to the shell. The shell is selected such that no residual masses are present at the location of the computation point. In this study we model the topographic masses (including bathymetry and ice sheets, cf. section 3.2) in spherical approximation; thus, $\delta \vec{g}^{\,\mathrm{SH}}$ corresponds to the gravitational attraction of a spherical shell (often termed Bouguer shell), and $\delta \vec{g}^{\,\mathrm{RM}}$ corresponds to the spherical terrain correction [e.g., *Kuhn et al.*, 2009].

For the practical evaluation of $\delta \vec{g}$, in this study, we replace the topographic masses by a series of tesseroids in spherical approximation, which are further approximated by rectangular prisms with first-order mass

equivalence and identical vertical extension. The methodology and corresponding formulae are provided by, e.g., *Anderson* [1976], *Grüninger* [1990], *Kuhn* [2000], and *Heck and Seitz* [2007] and will be briefly outlined here.

Tesseroids in spherical approximation are spherical mass elements bounded by surfaces of constant geocentric latitude (φ_1, φ_2), longitude (λ_1, λ_2), and geocentric radii $(r_1 = R + H_1, r_2 = R + H_2)$ and can be considered as the *natural* mass element when using heights H (here from equation (1)) given on a regular geocentric latitude-longitude grid (Figure 1). The geometrical center $Q_0(\varphi_0, \lambda_0, r_0)$ and dimensions $(\Delta\varphi, \Delta\lambda, \Delta r)$ of the tesseroid are given by (cf. Figure 1)

$$\begin{aligned} \varphi_0 &= (\varphi_1 + \varphi_2)/2; \quad \Delta\varphi = \varphi_2 - \varphi_1 \\ \lambda_0 &= (\lambda_1 + \lambda_2)/2; \quad \Delta\lambda = \lambda_2 - \lambda_1 \\ r_0 &= (r_1 + r_2)/2; \quad \Delta r = r_2 - r_1 \end{aligned} \tag{5}$$

As the integral over m_n in equation (2) cannot be exactly solved for a tesseroid [cf. *Heck and Seitz*, 2007], we approximate the tesseroid by a rectangular prism centered at the same location Q_0 with its edges being parallel to the axes x', y', and z' of a topocentric coordinate system located at the center of the tesseroid's top surface $Q(\lambda_0, \varphi_0, r_2)$ which coincides with the center of the prism's top surface (cf. Figure 1). For first-order mass equivalence and identical heights the dimension of the prism is given by [e.g., *Anderson*, 1976; *Grüninger*, 1990; *Heck and Seitz*, 2007]:

$$\Delta x = r_0 \Delta\varphi; \quad \Delta y = r_0 \cos\varphi_0 \Delta\lambda; \quad \Delta z = \Delta r \tag{6}$$

We compute the gravitational attraction of the rectangular prisms based on the well-known analytical formulae as provided by, e.g., *Mader* [1951], *Nagy* [1966], *Nagy et al.* [2000], and *Nagy et al.* [2002] and modified to a numerically more stable expression shown in, e.g., *Kuhn* [2000] and *Heck and Seitz* [2007]. Within our numerical studies we only focus on the z component δg_z (the gravity disturbance) of the vector $\delta\vec{g}$ (cf. equation (3)) at the location of the computation point P (cf. Figure 1).

2.2. Spectral Domain Forward Modeling

The technique description is largely based on the work by *Hirt and Kuhn* [2012], but modified here to accommodate for the additional high-frequency spectral constituents beyond the bandwidth of the input topography.

2.2.1. Topographic Potential in the Spectral Domain

The key ingredients for spectral domain forward modeling are topographic height functions and their integer powers. We define the dimensionless topographic height function (THF) as ratio of the topographic height H and the reference radius R. The THF raised to arbitrary integer power $p (p \in \mathbb{N})$ then reads

$$H^{(p)} = \frac{H^p}{R^p} \tag{7}$$

in the spatial domain. The spectral domain representation of $H^{(p)}$, denoted here with $H^{(p)}_{nm} = \left(\overline{\mathrm{HC}}, \overline{\mathrm{HS}}\right)^{(p)}_{nm}$, is obtained through spherical harmonic analyses of the $H^{(p)}$. The $H^{(p)}_{nm}$ of the THF are thus related to their spatial domain counterpart $H^{(p)}(\varphi, \lambda)$ via

$$H^{(p)}(\varphi, \lambda) = \sum_{n=0}^{N_{\max}} \sum_{m=0}^{n} \left(\overline{HC}^{(p)}_{nm} \cos m\lambda + \overline{\mathrm{HS}}^{(p)}_{nm} \sin m\lambda\right) \overline{P}_{nm}(\sin\varphi) \tag{8}$$

where the maximum harmonic degree $N_{\max}$ is commonly set identical with the maximum degree $n_{\max}$ of the topography model, and thus considered independent of the integer power p, e.g.,

$$N_{\max} = n_{\max}. \tag{9}$$

The vast majority of past works on spectral domain forward modeling relies (implicitly) on equation (9); see the list of cited references in section 1. As novelty of this study, we here extend the spectral forward modeling technique by introducing $N_{\max}$ as a function of the integer power p for the THFs

$$N_{\max} = p n_{\max}, \tag{10}$$

and therefore,

$$H^{(p)}(\varphi, \lambda) = \sum_{n=0}^{p n_{\max}} \sum_{m=0}^{n} \left(\overline{\mathrm{HC}}^{(p)}_{nm} \cos m\lambda + \overline{\mathrm{HS}}^{(p)}_{nm} \sin m\lambda\right) \overline{P}_{nm}(\sin\varphi) \quad . \tag{11}$$

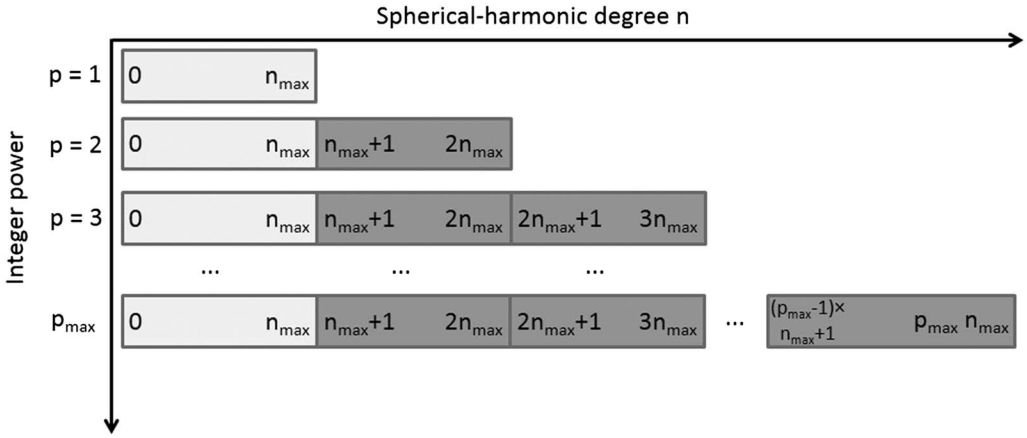

Figure 2. Contribution scheme for spectral domain gravity forward modeling: Contributions of integer powers p of the topography to the topographic potential as a function of the integer power (vertical axis) and the pth multiple of the input bandwidth (horizontal axis).

Increasing the maximum harmonic degree $N_{\max}$ from $n_{\max}$ to $pn_{\max}$ requires oversampling of the $H^{(p)}$ by factor p prior to computing the $H^{(p)}_{nm}$ via the spherical harmonic analyses. Compared to the maximum harmonic degree $n_{\max}$ of the topography model, twice the spectral resolution ($2n_{\max}$) is thus taken into account for the squared THF $H^{(2)}_{nm}$, and three times the resolution ($3n_{\max}$) for the cubed THF $H^{(3)}_{nm}$, and so forth.

The topographic gravitational potential (short: topographic potential) coefficients V_{nm} are calculated via a standard series expansion into powers p of the THFs $H^{(p)}_{nm}$ [after *Wieczorek*, 2007; *Hirt and Kuhn*, 2012]:

$$V_{nm} = \frac{1}{2n+1}\,\frac{4\pi R^3\rho}{M}\sum_{p=1}^{p\,\max}\frac{\prod_{i=1}^{p}(n+4-i)}{p!(n+3)}H^{(p)}_{nm} \tag{12}$$

where V_{nm} is the shorthand for the $\left(\overline{\mathrm{VC}},\overline{\mathrm{VS}}\right)_{nm}$ SHCs of the topographic potential, $p_{\max}$ is the maximum integer power of the series expansion, and M is the mass of the planet. From *Hirt and Kuhn* [2012, Figure 1; *Wieczorek*, 2007], the higher the resolution of the input topography $n_{\max}$, the more integer powers p must be taken into account in equation (12) for convergence. The number of terms also increases with the range of the heights relative to the reference radius R [see *Claessens and Hirt*, 2013]. For degree 2160 Earth topography mass models, it was shown that $p_{\max}=8$ yields truncation errors (resulting from dropping terms with $p>8$) well below the mGal level [cf. *Hirt and Kuhn*, 2012]. Another convergence analysis has shown truncation errors below the mGal level for degree 360 models and $p_{\max}=4$ [*Wieczorek*, 2007].

Equation (12) can easily be evaluated for individual integer powers p, instead of calculating the sum from $p=1$ to $p_{\max}$. Then, the contribution of the pth integer power of the topography to the topographic potential is obtained. Equation (12) can also be evaluated separately for harmonic band $n\in[\,0 \quad n_{\max}\,]$ and for pth multiples thereof: $n\in[\,(p-1)n_{\max}+1 \quad pn_{\max}\,]$. This leads to a new, generalized contribution scheme for spectral domain forward modeling shown in Figure 2.

The left column (light grey boxes in Figure 2) shows the contribution of the pth integer power of the topography limited to $n_{\max}$, these were investigated or calculated, e.g., by *Rummel et al.* [1988], *Tsoulis* [2001], *Wild-Pfeiffer and Heck* [2007], *Wieczorek* [2007], *Makhloof*, 2007, *Novák* [2010], *Balmino et al.* [2012], and *Hirt and Kuhn* [2012], among many others.

New are the columns with $n>n_{\max}$ (dark grey boxes in Figure 2). They reflect the additional high-frequency signals associated with forming powers of the THF. Raising the THF to power p =2 doubles the bandwidth of the input topography, and power p =3 triples the input bandwidth, leading to the triangular contribution scheme in Figure 2. This can be generalized to the statement "The p-th integer power of a topography expanded to spherical harmonic degree $n_{\max}$ contributes to the topographic potential up to degree p times $n_{\max}$."

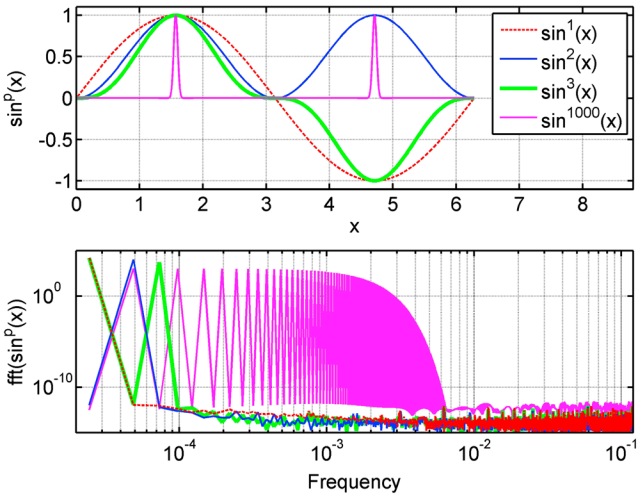

Figure 3. (top) Sine functions raised to integer powers $p = 1$, 2, 3, and 1000; (bottom) Fourier spectra (magnitudes) of the powered sine functions. Figure 3, bottom, exemplifies the gain in bandwidth as the power p increases. Variable x in radian, frequencies normalized to interval (0 1).

This finding can be easily verified by the frequencies present in the pth powers of sine or cosine functions (cf. Figure 3). For instance, raising the sine function with frequency f_0 to the second power doubles the frequency, e.g. $2f_0$, compared to the sine function. For the third power the maximum frequency present is $3f_0$ and so forth for higher powers (Figure 3). Raising the sine function to infinite power will result in an infinite sequence of equidistant delta functions of which the Fourier transform is also an infinite series of equidistant delta functions covering infinite multiples of f_0 [e.g., Brigham, 1988, p. 21]. This behavior is exemplified with a sine function raised to power $p = 1000$ in Figure 3.

Applying this analogy to the topography function H expressed through a series of sine and cosine functions (cf. equation (1)) covering the spectral band to a maximum degree n_{max}, e.g., $n \in [0 \quad n_{max}]$ the spectral band of the squared function extends to $2n_{max}$, as noted by *Heck and Seitz* [1991]. Ultimately, raising H to infinite power will result in a function covering the full spectrum even though the original function was band limited. This behavior can also be verified by analyzing the spectra of the powered THFs (section 3.3), thus confirming the contribution scheme. Further evidence in support of the contribution scheme is gathered by comparisons between gravity from space and spectral domain techniques (section 3.4).

2.2.2. Synthesis of Functionals of the Potential

The V_{nm} can be used to calculate the topographic potential or various functionals thereof in the spatial domain at the three-dimensional coordinates geocentric latitude φ, longitude λ, and geocentric radius r via spherical harmonic synthesis [e.g., *Holmes and Pavlis*, 2008; *Hirt*, 2012]. Here we evaluate the frequently used gravity disturbance δg (being the radial derivative of the gravitational potential, equivalent to δg_z introduced in section 2.1), defined through [after *Torge* 2001, p. 271]:

$$\delta g(\varphi, \lambda, r) = -\frac{\partial V}{\partial r} = \frac{GM}{r^2} \sum_{n=0}^{n\,\max} (n+1) \left(\frac{R}{r}\right)^n \sum_{m=0}^{n} \left(\overline{\mathrm{VC}}_{nm} \cos m\lambda + \overline{\mathrm{VS}}_{nm} \sin m\lambda\right) \bar{P}_{nm}(\sin\varphi). \tag{13}$$

As geocentric radius r of the evaluation points, we choose the surface of the topographic mass model, as represented through

$$r = r(\varphi, \lambda) = R + H(\varphi, \lambda) \tag{14}$$

This is done in order to account for the effect of gravity attenuation with height [cf. *Hirt*, 2012]. For reasons outlined in *Hirt* [2012] and *Hirt and Kuhn* [2012], evaluation of equation (13) in terms of dense grids can be computationally demanding when the radii of evaluation $r(\varphi, \lambda)$ vary along parallels (φ = constant), as in equation (14). A numerically efficient and precise approximate solution is obtained here via field continuation of gravity disturbances with higher-order gradients of δg [*Hirt and Kuhn*, 2012]

$$\delta g^{\,k\,\max}(\varphi, \lambda, r) \approx \sum_{k=0}^{k\,\max} \frac{1}{k!} \left.\frac{\partial^k \delta g}{\partial r^k}\right|_{r = R + H_{\mathrm{ref}}} (H - H_{\mathrm{ref}})^k \tag{15}$$

where k_{max} is the maximum order of the series expansion, H_{ref} is some mean reference height for acceleration of convergence, and $\partial^k \delta g/\partial r^k$ is the kth order radial derivative of δg calculated at a constant height $r = R + H_{ref}$ via [*Hirt*, 2012]

$$\frac{\partial^k \delta g}{\partial r^k} = (-1)^k \frac{GM}{r^{k+2}} \sum_{n=0}^{n\,max} (n+1) \left\{ \prod_{i=1}^{k} (n+i+1) \right\} \left(\frac{R}{r} \right)^n \cdot \sum_{m=0}^{n} \left(\overline{VC}_{nm}^{p\,max} \cos m\lambda + \overline{VS}_{nm}^{p\,max} \sin m\lambda \right) \overline{P}_{nm}(\sin\varphi). \quad (16)$$

3. Numerical Study

3.1. General

A numerical study is carried out based on the publicly available RET2012 topography model (section 3.2) with the goals to analyze the spectra of the THFs (section 3.3.1) and of their contributions to the topographic potential (section 3.3.2) in order to investigate the signal strengths of these contributions for gravity disturbances in the spatial domain. The study then systematically compares gravity disturbances from spatial and spectral domain forward modeling as a function of the pth integer power contributions and maximum harmonic degree $N_{max} = pn_{max}$ taken into consideration (section 3.4). A main motivation for the numerical study is the verification of the contribution scheme for spectral domain forward modeling (Figure 2).

For the spherical harmonic synthesis of the topography H (equation (1)), and analyses of the THFs $H_{nm}^{(p)}$ (equation (7)), we use the SHTools package (www.shtools.org), and for spherical harmonic synthesis of gravity disturbances and their kth order radial derivatives (cf. equation (16)) a modification of the harmonic_synth software [*Holmes and Pavlis*, 2008]. Both packages deploy the routines by *Holmes and Featherstone* [2002] for the stable computation of the associated Legendre functions $\overline{P}_{nm}(\sin\varphi)$ to degree $n = 2700$. Given that the $\overline{P}_{nm}(\sin\varphi)$ are subject to numerical instabilities which increase for $n > 2700$ [*Holmes and Featherstone*, 2002], we confine all of our numerical tests to

$$N_{max} = pn_{max} \leq 2700. \quad (17)$$

As a consequence, the bandwidth $[0 \quad n_{max}]$ of the input topography must be chosen sufficiently narrow to allow for accurate evaluation of the high-frequency p multiples of $[0 \quad n_{max}]$. Among many possible bandwidths, we have chosen the input band $[0 \quad n_{max} = 360]$ as our example for band-limited topographic mass models. For this band, calculation and analyses of multiples of the input band $[0 \quad n_{max} = 360]$ up to $p = 7$ are safely possible. As will be shown, this is sufficient to verify the contribution scheme in Figure 1.

We acknowledge that algorithms for the stable computation of $\overline{P}_{nm}(\sin\varphi)$ to arbitrary degree have been developed [*Fukushima*, 2012a, 2012b], which could be used in a future case study to ultrahigh degree, once tested implementations for spherical harmonic analyses become available (for spherical harmonic synthesis software to ultrahigh degree see, e.g., *Bucha and Janák* [2013]).

3.2. Data and Constants

As model representing the topographic masses, we use the freely available spherical harmonic data set RET2012 (rock-equivalent topography model) of Curtin University's Earth2012 model suite (URL: http://geodesy.curtin.edu.au/research/models/Earth2012/, file Earth2012.RET2012.SHCto2160.dat). This allows replication of our study. Based on a range of input data sets, RET2012 represents the masses of the visible topography, of the oceans and major inland lakes, and major ice sheets using a single-constant mass density of $\rho = 2670\ \mathrm{kg\,m^{-3}}$. Rock-equivalent heights of ice and water masses were derived through mathematical compression into rock-equivalent mass layers [e.g., *Rummel et al*., 1988], see *Hirt et al*. [2012] and *Hirt* [2013] for details on the procedures applied to generate the RET2012 SHCs H_{nm}. Though the SHCs of RET2012 are available to degree and order 2160, we use this model only from degree and order 0 to degree and order 360 ($= n_{max}$). As such, only the RET2012 spectral band of harmonic degrees 0 to 360 defines the input (source) topography in this study.

For our tests of the two forward modeling techniques, we use exactly the same topographic mass model as input: In the spatial domain technique heights $H(\varphi, \lambda)$ synthesized from the RET2012SHCs H_{nm} at various resolutions, and in the spectral domain technique the H_{nm} directly as input topography. Also used with

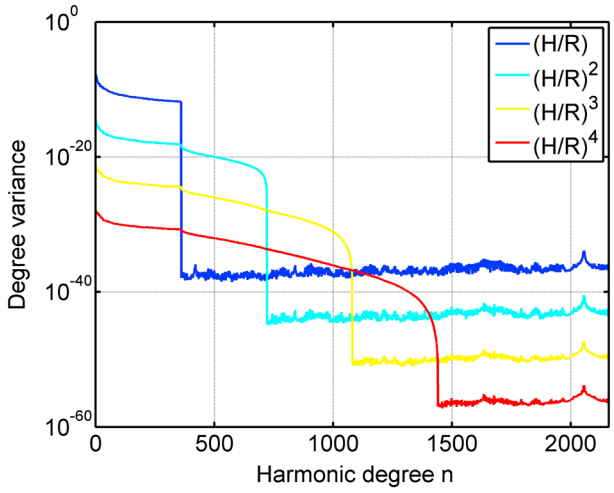

Figure 4. Degree variances of the first four integer powers p of the topographic height function (H/R) band limited to degree 360.

identical numerical values in both techniques are the topographic mass density $\rho = 2670\ \mathrm{kg\,m^{-3}}$, reference radius $R = 6{,}378{,}137$ m (semimajor axis of GRS80) [*Moritz*, 2000], the universal gravitational constant $G = 6.67384 \times 10^{-11}\ \mathrm{m^3\,kg^{-1}\,s^{-2}}$ [*Mohr et al.*, 2012, p. 72], and total Earth's mass (including atmosphere) $M = 5.9725810 \times 10^{24}$ kg (from the *GM* product of GRS80 [*Moritz*, 2000]).

3.3. Spectral Analyses

3.3.1. Topography

To derive the spectra of the THFs, we (i) synthesized RET2012 heights H in spectral band $[0 \quad n_{\max} = 360]$ in terms of regularly spaced geocentric latitude-longitude grid of 2 arc min resolution ($5400 \times 10{,}800$ heights), (ii) normalized this grid with R, (iii) raised the resulting THFs to integer power $p \geq 1$, and (iv) analyzed harmonically the powered THFs $H^{(p)}$ with SHTools (algorithm by *Driscoll and Healy* [1994]). This procedure gave us the $H^{(p)}_{nm}$-SHCs to a maximum degree and order $n = m = 2700$. Note that the THFs assume very small values as the power increases (e.g., $p = 5$, THF $\approx 10^{-20}$ for heights around 1 km). To avoid possible numerical problems in the analysis associated with small numbers, we scaled each THF with its maximum value before the analysis and undid this scaling at coefficient level. The dimensionless degree variances of the THFs

$$\sigma H_n^{(p)2} = \sum_{m=1}^{n} \left(\overline{\mathrm{HC}}_{nm}^{(p)2} + \overline{\mathrm{HS}}_{nm}^{(p)2} \right) \tag{18}$$

are shown in Figure 4 as a function of the degree n for the first four integer powers. For the linear THF $H^{(1)}$, the spectrum slowly decays from degree 0 to degree 360, drops by 25 orders of magnitude at degree 361, and stays at the level of $\sim 10^{-37}$ for all other degrees (noise level as given by the computational precision). This behavior is expected, given the bandwidth limitation of the input topography to $n_{\max} = 360$. The squared THF $H^{(2)}$ is smaller in amplitude so features less power than $H^{(1)}$. The spectrum of $H^{(2)}$ slowly decays to degree 360, drops slightly around degree 361, and experiences another slow decay up to degree 720, before falling to noise level. This behavior shows that the bandwidth of $H^{(2)}$ is extended by factor 2 compared to the input band (through rising to power 2). Figure 4 further shows for the cubed THF $H^{(3)}$ significant spectral power in band 0 to 1080 (3 times the input bandwidth) and for $H^{(4)}$ significant spectral power to degree 1440 (4 times the input bandwidth). Exemplified with the first four integer powers of the THFs, Figure 4 nicely shows the increase in bandwidth by a factor of p with respect to the input band limitation to $n_{\max} = 360$.

3.3.2. Potential

We separately evaluated equation (12) for powers $p = 1$ to 6, giving us the pth contribution of the topography to the topographic potential $V^{(p)}_{nm}$. The dimensionless potential degree variances

$$\sigma V_n^{(p)2} = \sum_{m=1}^{n} \left(\overline{\mathrm{VC}}_{nm}^{(p)2} + \overline{\mathrm{VS}}_{nm}^{(p)2} \right) \tag{19}$$

are shown in Figure 5, as well as the degree variances of the total topographic potential $V^{p\,\max=6}_{nm}$ (sum of the six contributions $V^{(p)}_{nm}$). As expected from Figure 4, the contribution made by $p = 1$ only possesses power to $n_{\max} = 360$, while the other five integer powers contribute to degree 720 ($p = 2$), to 1080 ($p = 3$), all the way to degree ~2160 ($p = 6$). Assuming that degree variances below the level of about $\sim 10^{-27}$ are negligible [see *Hirt and Kuhn*, 2012], Figure 5 suggests that the powers $p = 2$ to 5 contribute significantly to $V^{p\,\max=6}_{nm}$ in band $[361 \quad 720]$ and powers $p = 3$ to 4 in band [721 1080]. The higher-order contributions of a band-limited topography to the topographic potential tend to contribute largest well beyond the initial input bandwidth, as is seen from the degree variances for $p = 6$, which are maximum near degree ~700, though originating from a topography band limited to $n_{\max} = 360$.

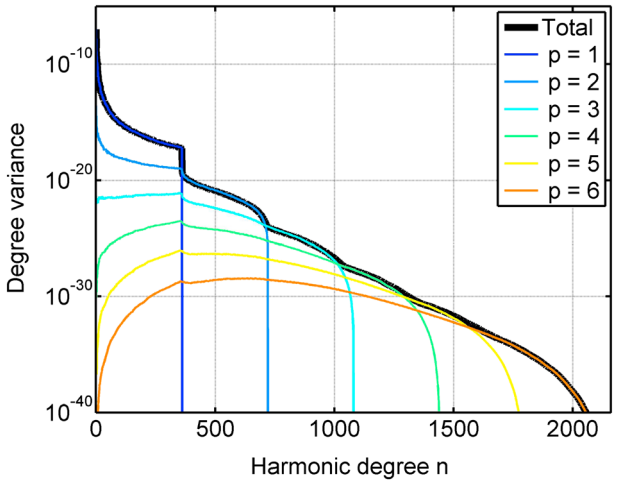

Figure 5. Potential degree variances of the contributions made by the first six integer powers of the topography to the topographic potential (blue to orange) and of potential degree variances of the (resulting) total topographic potential (black line). Topography is band limited to degree and order 360.

3.4. Spatial Analyses

This section compares gravity disturbances from spatial forward modeling (section 2.1) and from spectral forward modeling (section 2.2) over the Himalaya test region ($25° < \varphi < 35°$ and $85° < \lambda < 95°$). Because of the most rugged topography and thus gravitational field, this area should serve as a "worst case" test area for the technique comparison. Common to the application of both techniques is the dense computation point spacing of 1 arc min, as well as the arrangement of computation points at the surface of the topography H. This takes into account attenuation of gravity with height. Over areas where $H < 0$, the computation is carried out at $H = 0$ (avoiding computations inside the reference sphere).

In the spatial domain forward modeling, topographic mass effects induced by the global topography were analytically computed using the discretized Newtonian integration approach described in section 2.1. Heights from the topography model were synthesized over the test area in terms of densely spaced grids (20 arc sec resolution) in spectral band $[0 \quad n_{max} = 360]$. As such, the grid of topographic heights is highly oversampled by a factor of 90 (note that the maximum harmonic degree of 360 corresponds to a formal spatial resolution of 1800 arc sec or ~50 km at the equator). In other words, the spherical harmonic topography is very well represented in the space domain through dense grid point spacing. This oversampling minimizes discretization errors in spatial domain forward modeling.

To reduce computation times, a number of grid resolutions were used as follows: 20 arc sec within 1° radius, 1 arc min within 3° radius and 3 arc min beyond. Because of the quadratic attenuation of gravity with distance, the use of lower grid resolutions outside some radius is common practice [e.g., *Forsberg* [1984]] and—if selected properly—results in approximation errors well below one μGal. Figure 6 shows the gravity disturbances from input band $[0 \quad n_{max} = 360]$ over our test area, as obtained from the spatial forward modeling (Newtonian integration).

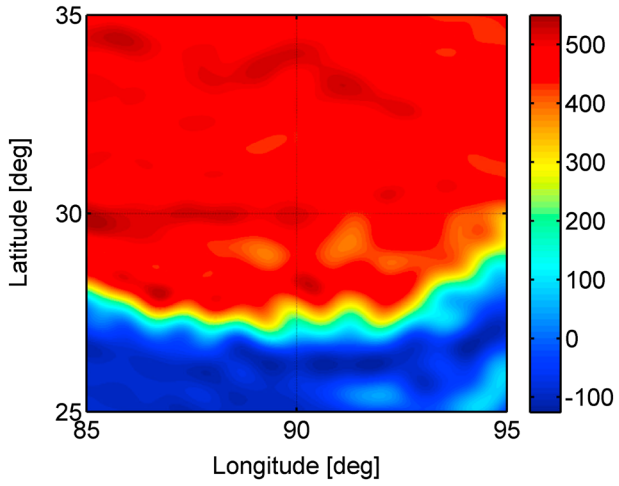

Figure 6. Topographic gravity over the Himalaya test area from space domain gravity forward modeling (Newton integration), topographic input bandwidth limited to degree and order 360, and unit in mGal ($= 10^{-5}$ m s^{-2}).

Following the contribution scheme of spectral forward modeling, we computed gravity disturbances as a function of (i) the integer power p and of (ii) the bandwidth

$$[0 \quad n_{max}], \quad p = 1$$

$$[(p-1)n_{max} + 1 \quad pn_{max}], \quad p > 1,$$

respectively. The calculation of each individual contribution made by the topography to the topography-implied gravity disturbance is based on continuation with higher-order gravity gradients to $k_{max} = 10$ and an average reference height $H_{ref} = 3000$ m (equations (15) and (16)). From a comparison with gravity from direct 3-D spherical

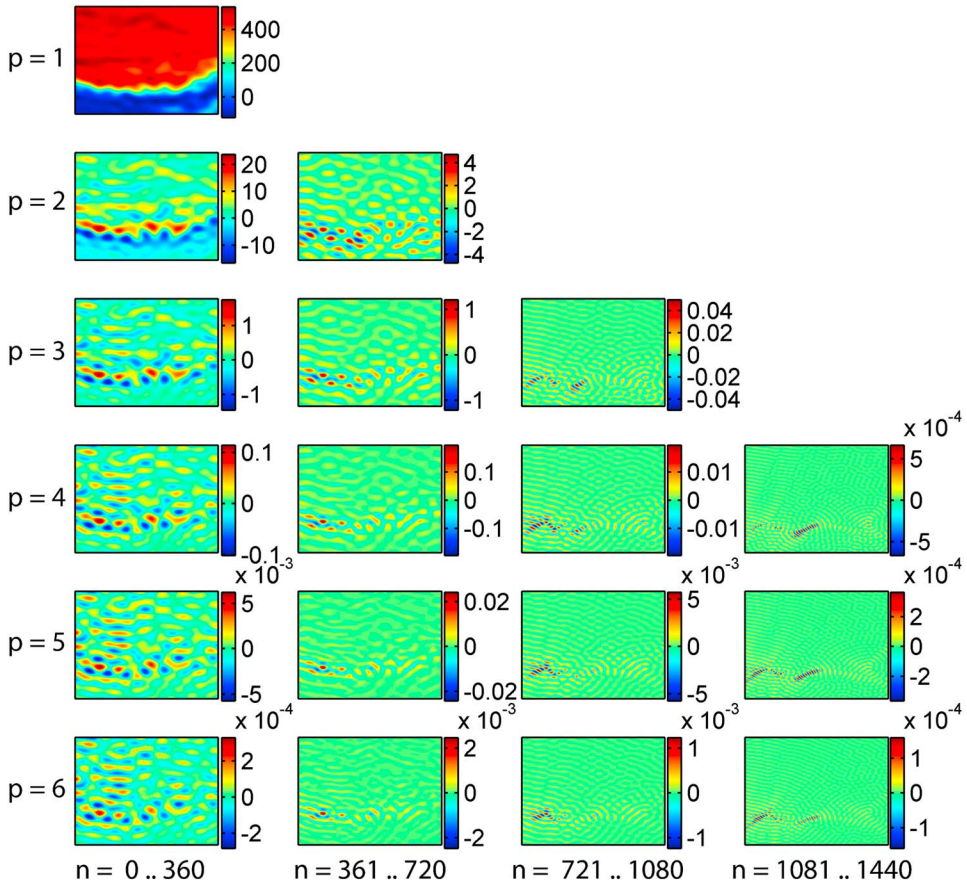

Figure 7. Single contributions of the topography to the topographic gravity over the Himalaya area ($25° < \varphi < 35°$, $85° < \lambda < 95°$) as a function of the integer power p (increasing from top to bottom), and of the pth multiple of the input band (increasing from left to right). Input band is limited to harmonic degree 360, unit in mGal.

harmonic synthesis (equation (13)) at the surface of the topography, approximation errors were below 0.1 μGal (tested for $p_{max} = 6$ and $N_{max} = 1440$), so safely negligible.

The spectral contributions of the topography to the gravity disturbance are displayed in Figure 7 over our test area, whereby the arrangement of panels follows the scheme introduced in Figure 2. The bulk of the gravity signal originates from the linear term ($p = 1$) evaluated to $n_{max} = 360$. It is seen that from $p = 1$ to 4 the contributions gradually decrease to the 0.1 mGal level and diminish for higher-order powers. The three columns to the right show the topography-implied signals in bands [361 720], [721 1080], and [1081 1440]. These are all multiples of the input bandwidth which were not considered in previous "traditional" spectral domain forward modeling. From Figure 7, the squared and cubed topography generates gravity signals larger than 1 mGal, both within and beyond the input band limitation $n_{max} = 360$. Contributions larger than 10 μGal are made by $p = 1$ to 5 in band [361 720], and $p = 3$ to 4 in band [721 1080], while the contributions associated with band [1081 1440] are below the 1 μGal level. Qualitatively, this is in good agreement with the spectral analyses made in section 3.3.2.

As the central result of this study, Figure 8 shows the differences between gravity disturbances from spectral domain and spatial domain forward modeling as a function of the maximum integer power p_{max} used in equation (12) and the maximum harmonic degree $N_{max} = pn_{max}$ evaluated in the spectral domain. The arrangement of panels follows Figure 7, but the spectral contributions are accumulated, i.e., sums computed to p_{max} and N_{max}. Selected descriptive statistics (root-mean-square and maximum absolute value of the difference) are reported in Table 1. From Figure 8 and Table 1, the agreement among the two techniques improves with increasing p_{max} and increasing N_{max}, from ~5 mGal root-mean-square (RMS) (31 mGal maximum difference) for $p_{max} = 1$ and $N_{max} = n_{max} = 360$ to an excellent level of 0.3 μGal RMS (~2 μGal maximum difference) for $p_{max} = 6$ and $N_{max} \geq 1080$, see Table 1.

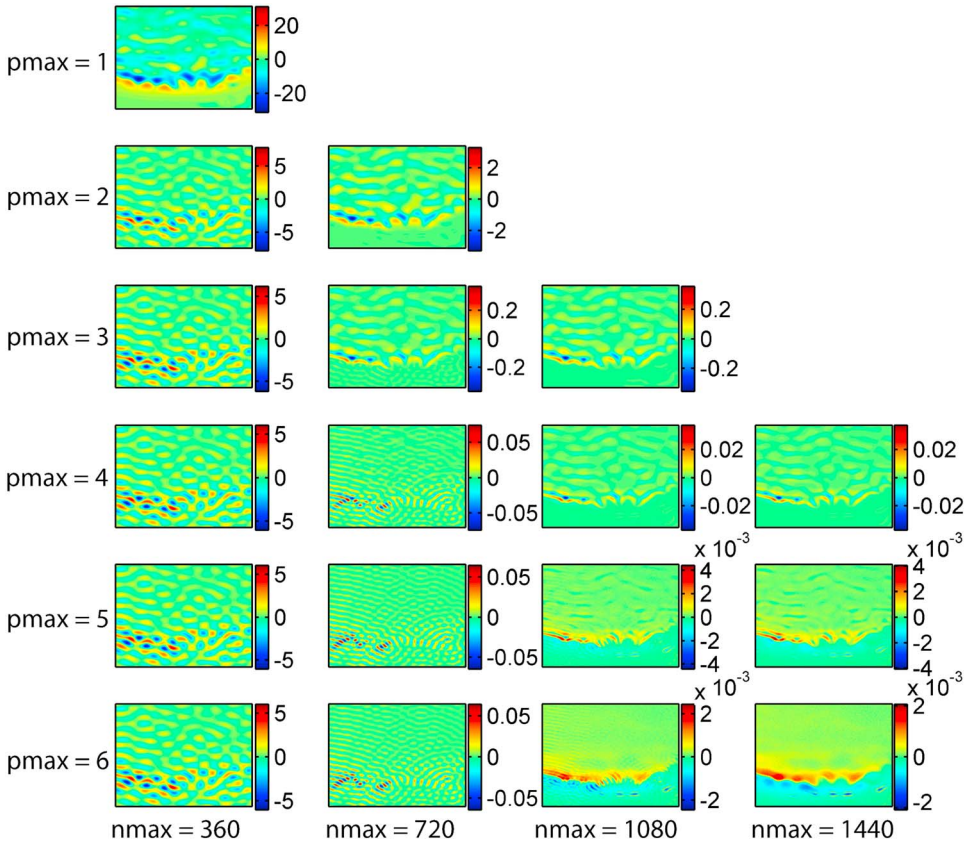

Figure 8. Residuals between topographic gravity from spatial and spectral forward modeling as a function of (i) maximum integer power p_{max} (increasing from top to bottom) and (ii) maximum harmonic degree N_{max} (increasing from left to right) used in the spectral domain forward modeling. Figure should be read together with Figure 7. Differences are in the sense spectral minus spatial modeling, units in mGal.

Focusing on the left column ($N_{max} = n_{max} = 360$), in Figure 8, the discrepancies among the two techniques always exceed 5 mGal, irrespective of the p_{max} chosen. The residuals in the left column thus correspond to a traditional comparison between spectral and spatial forward modeling with spectral consistency among topography and gravity presumed. Most importantly, it is the consideration of multiples of the input bandwidth that improves the agreement by a factor of ~100 to the 50 μGal level ($N_{max} = 2n_{max} = 720$), and by another factor of ~25 to the μGal level ($N_{max} = 3n_{max} = 1080$), also see Table 1.

The comparisons demonstrate that the Newtonian integration inherently "captures" the additional high-frequency signals (beyond n_{max}), without explicit modeling as must be done in the spectral domain. The remaining discrepancies are likely to reflect numerical integration errors in the spatial domain technique. Further, the comparisons also show (implicitly) sufficient convergence of the series expansions applied for field continuation (equations (15) and (16)).

Table 1. Residuals Between Spectral and Spatial Domain Forward Modeling[a]

	$N_{max} = 360$	$N_{max} = 720$	$N_{max} = 1080$	$N_{max} = 1440$
$p_{max} = 1$	5.43(31.34)	na	na	na
$p_{max} = 2$	1.03(7.83)	0.38 (3.30)	na	na
$p_{max} = 3$	0.96(6.17)	0.03 (0.37)	0.03 (0.36)	na
$p_{max} = 4$	0.96(6.06)	7.6×10^{-3} (7.5×10^{-2})	2.5×10^{-3} (3.8×10^{-2})	2.5×10^{-3} (3.8×10^{-2})
$p_{max} = 5$	0.96(6.06)	7.3×10^{-3} (6.5×10^{-2})	4×10^{-4} (4.4×10^{-3})	4×10^{-4} (4.1×10^{-3})
$p_{max} = 6$	0.96(6.06)	7.3×10^{-3} (6.4×10^{-2})	4×10^{-4} (2.5×10^{-3})	3×10^{-4} (2.1×10^{-3})

[a]Reported are the root-mean-square and in brackets the maximum absolute difference between gravity from the two techniques, unit in mGal. Not applicable = na.

3.5. Computational Costs

Regarding the computational costs for spectral domain forward modeling, a spherical harmonic analysis of a single power of the THF took ~3 min on a standard office PC (input topography band limited to degree 360 and output coefficients of the THF to degree 2160). With the first six powers of the THF taken into account (Figure 5), the overall computation time for application of the contribution scheme (Figure 2) and synthesis of gravity effects with gradients over our $10° \times 10°$ study area (360,000 points) was less than 1 h. Opposed to this, the Newton integration required more than 10,000 CPU hours on Western Australia's iVec supercomputer to provide gravity effects over the same area. The computational costs of the space domain technique were relatively high because of the oversampling (20 arc sec grid resolution for a degree 360 signal) that was chosen to reduce discretization errors down to the μGal level. Polyhedral bodies instead of prisms may not require such extreme oversampling to yield similarly low discretization errors, thus reducing the computational cost.

While in the case study the spectral technique was numerically more efficient than the spatial technique, there is a clear tendency of the spectral method becoming much more computationally intensive as the degree increases. Application of the contribution scheme in Figure 2 for a source topography model to degree 2160 (10 km resolution) would require multiple harmonic synthesis, e.g., to degree and order 10,800 (5 times oversampling) to capture the short-scale gravity signals at spatial scales less than 10 km. Currently, there is no software at hand to accurately gauge the computational costs for this or other high-degree applications of the contribution scheme. Importantly, increasing the spectral resolution will increase the computation times for spectral forward modeling but not for the Newton integration if the above grid resolutions remain the same.

4. Discussion

Gravity disturbances obtained from two entirely independent modeling techniques, but from the same input mass distribution, were compared over a worst case test area, with special focus on the spectral domain contributions made by (i) the integer powers p of the topography and (ii) multiples p of the input bandwidth. Our numerical tests unambiguously demonstrate that a band-limited topographic mass distribution implies a gravitational field with spectral power far beyond the input band limitation to n_{max}. Our test procedures were sensitive enough to empirically show the relevance of the first three multiples ($N_{max} = 4n_{max}$) of the input band, as well as of higher-order contributions up to $p = 6$. This provides strong evidence for the validity of the contribution scheme introduced in Figure 2, and thus justifies the statement that a band-limited topography generates (in good approximation) a full-spectrum gravity field.

The discrepancies among gravity from the spectral and spatial techniques were found to be smaller than ~2 μGal when integer power contributions to $p_{max} = 6$ were evaluated, and the bandwidth of the potential was extended by a factor 4 over the bandwidth of the topography ($N_{max} = 4n_{max}$). With a maximum signal strength of ~500 mGal (Figure 6), this translates into a relative error of 4×10^{-6}. To our knowledge, such a low relative error among the two forward modeling techniques has not yet been reported in the literature. Compared to the uncertainty of the universal gravitational constant G of about 1.2×10^{-4} [*Mohr et al.*, 2012, p. 72], these technique discrepancies play a diminishing role for the accurate computation of topography-generated gravity. All in all, the level of agreement between the forward modeling techniques can be considered as excellent.

Holistically, our numerical comparisons provide valuable mutual feedback on the two techniques applied, contributing to a better understanding of gravity forward modeling. In particular, the comparisons demonstrate the following:

1. The importance of the computation point height. For the meaningful calculation of gravity disturbances (or other functionals of the potential), computation points in both techniques were located at the topography (other locations are possible). While the attenuation of gravity with height and distance from the generating masses is accounted for through the choice of computation points in the Newtonian integration, consideration is possible in the spectral domain through gravity synthesis at the surface of the topography. The excellent agreement between gravity from the two techniques (Table 1) implicitly shows convergence of the gradient solution applied here (equations (16) and (17)).

2. The importance of higher-order integer contributions. For the accurate application of spectral domain forward modeling higher-order contributions made by integer powers of the topography become increasingly relevant as the resolution of the input topography increases [see also *Hirt and Kuhn*, 2012]. While the theory [e.g., *Rummel et al*., 1988; *Wieczorek and Phillips*, 1998] clearly shows the need for higher-order contributions, there are only few studies concerned with empirical verification of these terms based on independent or external methods. *Chambat and Valette* [2005] showed the relevance of the squared topographic contribution (via a comparison with geopotential models). Our technique comparisons now demonstrate the relevance of integer powers up to the sixth power.
3. The importance of multiples of the input bandwidth. To accurately compute the gravitational field implied by a topographic mass distribution in the spectral domain, the contributions of the higher-order powers must be calculated in multiples of the input bandwidth. The additional high-frequency gravity signals are significant (in our tests up to 4 times the input bandwidth), as was shown by comparison with the independent Newtonian integration.

When the additional high-frequency signals remained (deliberately) unmodeled in our study (i.e., $N_{max} = n_{max}$), the discrepancies among the two techniques would translate into relative errors of ~1% ($N_{max} = n_{max} = 360$, cf. Table 1), but this will be larger for $N_{max} = n_{max} > 360$. Not shown here for the sake of brevity, but a second numerical test with input band $N_{max} = n_{max} = 2160$ yielded ~6.5% relative errors (34 mGal maximum discrepancy among both techniques versus ~530 mGal signal) when neglecting signals beyond the input bandwidth in the spectral technique. These magnitudes are comparable with relative errors encountered in other studies comparing spectral and spatial forward modeling (0.8% [*Novák and Tenzer*, 2013]; 3% [*Kuhn and Seitz*, 2005]; 4.5% [*Wild-Pfeiffer and Heck*, 2007], and ~10% [*Wang et al*., 2010]; *Balmino et al*., 2012]; please see section 1). Given our relative errors are at the level of 10^{-4} (0.01%) for $N_{max} = 2n_{max} = 720$ and diminish to the level of 4×10^{-6} (0.0004%) for $N_{max} = 4n_{max} = 1440$, it is safe to conclude that (unmodeled and usually truncated) topography-generated gravity signals beyond n_{max} are key candidates for the discrepancies among spectral and spatial forward modeling encountered in the aforementioned studies.

Wieczorek [2007] noted in his review paper on the character of the spectral forward modeling equation (equation (12) in this paper): "While the sum of Eq. 30 [*Wieczorek*, 2007, p 19] is finite, and hence exact, the number of terms grows linearly with spherical harmonic degree." However, our results and the contribution scheme (Figure 2) show that the sum used by *Wieczorek* [2007] cannot be used for the exact computation of gravity implied by a given topography, because spectral consistency among gravity and topography is assumed when using $N_{max} = n_{max}$. Rather, the *exact* calculation of gravity from topography by harmonic expansion requires consideration of $N_{max} = p_{max} n_{max}$ (equation (10)), as shown in this study.

5. Conclusions

This paper has investigated the spectral (bandwidth) inconsistency among spherical harmonic topographic mass models and the generated gravitational field. A generalized contribution scheme was introduced for the spectral domain forward modeling technique as a function of integer powers and multiples of the input topography's bandwidth. This new scheme mathematically describes the extension of the spectrum associated with the transformation of topography to gravity based on Newton's law of gravitation. The short-scale gravity signals generated by a band-limited topography can be surprisingly easily modeled in the spectral domain as shown in this paper. The validity of the contribution scheme was confirmed through spectral analyses and space domain comparisons.

Modeling the additional high-frequency signals beyond the input bandwidth has brought together the spatial domain and spectral domain forward modeling technique from a level of 10^{-2} to the level of better than 10^{-5} in terms of gravity disturbances. This is a considerable improvement by 3 orders of magnitude.

There are applications where the spectral inconsistency between topographic mass models and gravitational potential is entirely uncritical, for instance comparisons between observed and topography-implied gravitational fields in spherical harmonics (as in the calculation of spherical harmonic Bouguer gravity). This is because the fields are spectrally consistent in the gravity domain.

However, if the gravitational field generated by a spherical harmonic topography is to be exactly calculated, then multiples of the input topography's bandwidth should be computed and evaluated in the spectral domain. Multiples of the input bandwidth can be expected to become more relevant as the resolution increases (cf. section 4). This has important implications for present and future ultrahigh-degree models of the topographic potential: For a standard degree 2160 topography model, the implied topographic potential would have to be modeled to (a coarsely estimated) degree of ~10,800 or higher if sufficient consistency between the two quantities is sought. For an input bandwidth of a topography model to degree and order 10,800 [e.g., *Balmino et al*., 2012] would require spectral domain modeling to extremely high degree to accurately compute the generated gravitational potential.

Finally, with the understanding of the spectral domain technique drawn from this study, comparisons among spectral domain and spatial domain forward modeling can now be much better utilized for a mutual validation of forward modeling software implementations and detailed testing of forward modeling approaches. For instance, this can be helpful for (i) testing integration formulas for gravity effects from mass bodies [*Grombein et al*., 2013; *D'Urso*, 2014] in the spatial domain technique or (ii) investigating the convergence behavior of series expansions in the spectral domain in some not entirely undisputed cases (e.g., evaluations inside the masses or inside the reference body).

Acknowledgments

We thank the Australian Research Council (ARC) for funding through discovery project grant DP120102441. This study was partially supported by Technische Universität München (TUM), Institute for Advanced Study (IAS), funded by the German Excellence Initiative and the European Union Seventh Framework Programme under grant agreement 291763. Christian Hirt is the recipient of an ARC DORA award and a TUM/IAS Hans-Fischer Fellowship. Mark Wieczorek is thanked for advice on his SHTools software package and Sten Claessens for the hint on the GRS80 reference field being an analogy to our work. We thank two reviewers for their valuable comments on our manuscript and the Editor for the manuscript handling. Western Australia's iVec supercomputing facility (www.ivec.org) was used for parts of the calculations presented in this work.

References

Anderson, E. G. (1976), The effect of topography on solutions of Stokes' problem, Unisurv S-14 report, School of Surveying, University of New South Wales, Kensington, Australia.

Bagherbandi, M., and L. E. Sjöberg (2012), A synthetic Earth gravity model based on a topographic-isostatic model, *Stud. Geophys. Geod.*, *56*(2012), 935–955, doi:10.1007/s11200-011-9045-1.

Balmino, G., N. Vales, S. Bonvalot, and A. Briais (2012), Spherical harmonic modelling to ultra-high degree of Bouguer and isostatic anomalies, *J. Geod.*, *86*(7), 499–520, doi:10.1007/s00190-011-0533-4.

Benedek, J. (2004), *The Application of Polyhedron Volume Elements in the Calculation of Gravity Related Quantities*, Special Issue of Österreichische Beiträge zu Meteorologie und Geophysik, vol. 31, pp. 99–106.

Brigham, E. O. (1988), *The Fast Fourier Transform and Its Applications*, 448 pp., Prentice Hall, N. J.

Bucha, B., and J. Janák (2013), A MATLAB-based graphical user interface program for computing functionals of the geopotential up to ultra-high degrees and orders, *Comput. Geosci.*, *56*, 186–196, doi:10.1016/j.cageo.2013.03.012.

Chambat, F., and B. Valette (2005), Earth gravity up to second order in topography and density, *Phys. Earth Planet. Inter.*, *151*(1-2), 89–106, doi:10.1016/j.pepi.2005.01.002.

Claessens, S. J., and C. Hirt (2013), Ellipsoidal topographic potential—New solutions for spectral forward gravity modelling of topography with respect to a reference ellipsoid, *J. Geophys. Res. Solid Earth*, *118*, 5991–6002, doi:10.1002/2013JB010457.

Driscoll, J. R., and D. M. Healy (1994), Computing Fourier transforms and convolutions on the 2-sphere, *Adv. Appl. Math.*, *15*, 202–250.

D'Urso, M. G. (2014), Analytical computation of gravity effects for polyhedral bodies, *J. Geod.*, *88*(1), 13–29, doi:10.1007/s00190-013-0664-x.

Eshagh, M. (2009), Comparison of two approaches for considering laterally varying density in topographic effect on satellite gravity gradiometric data, *Acta Geophys.*, *58*(4), 661–686, doi:10.2478/s11600-009-0057-y.

Forsberg, R. (1984), A study of terrain reductions, density anomalies and geophysical inversion methods in gravity field modelling, report 355, Department of Geodetic Science and Surveying, Ohio State Univ., Columbus, Ohio.

Fukushima, T. (2012a), Numerical computation of spherical harmonics of arbitrary degree and order by extending exponent of floating point numbers, *J. Geod.*, *86*(4), 271–285, doi:10.1007/s00190-011-0519-2.

Fukushima, T. (2012b), Numerical computation of spherical harmonics of arbitrary degree and order by extending exponent of floating point numbers: II First-, second-, and third-order derivatives, *J. Geod.*, *86*(11), 1019–1028, doi:10.1007/s00190-012-0561-8.

Grombein, T., K. Seitz, and B. Heck (2013), Optimized formulas for the gravitational field of a tesseroid, *J. Geod.*, *87*(7), 645–660, doi:10.1007/s00190-013-0636-1.

Gruber C., P. Novák, F. Flechtner, and F. Barthelmes (2013), Derivation of the topographic potential from global DEM models, in *International Association of Geodesy Symposia*, vol. 139, pp. 535–542, Springer-Verlag, Berlin Heidelberg, doi:10.1007/978-3-642-37222-3__71.

Grüninger, W. (1990), Zur topographisch-isostatischen Reduktion der Schwere, PhD thesis, Universität Karlsruhe.

Jacoby, W., and P. L. Smilde (2009), *Gravity Interpretation*, Springer, Berlin and Heidelberg.

Heck, B., and K. Seitz (1991), Nonlinear effects in the scalar free geodetic boundary value problem, spherical harmonic representation of the effects on the reduced boundary condition, the disturbing potential and the vertical position correction, report, 78 pages, Institute of Geodesy, University of Stuttgart, ISSN 0933-2839.

Heck, B., and K. Seitz (2007), A comparison of the tesseroid, prism and point-mass approaches for mass reductions in gravity field modelling, *J. Geod.*, *81*(2), 121–136, doi:10.1007/s00190-006-0094-0.

Hirt, C., U. Marti, B. Bürki, and W. E. Featherstone (2010), Assessment of EGM2008 in Europe using accurate astrogeodetic vertical deflections and omission error estimates from SRTM/DTM2006.0 residual terrain model data, *J. Geophys. Res.*, *115*, B10404, doi:10.1029/2009JB007057.

Hirt, C., M. Kuhn, W. E. Featherstone, and F. Göttl (2012), Topographic/isostatic evaluation of new-generation GOCE gravity field models, *J. Geophys. Res.*, *117*, B05407, doi:10.1029/2011JB008878.

Hirt, C., and M. Kuhn (2012), Evaluation of high-degree series expansions of the topographic potential to higher-order powers, *J. Geophys. Res.*, *117*, B12407, doi:10.1029/2012JB009492.

Hirt, C. (2012), Efficient and accurate high-degree spherical harmonic synthesis of gravity field functionals at the Earth's surface using the gradient approach, *J. Geod.*, *86*(9), 729–744, doi:10.1007/s00190-012-0550-y.

Hirt, C. (2013), RTM gravity forward-modeling using topography/bathymetry data to improve high-degree global geopotential models in the coastal zone, *Marine Geod.*, *36*(2), 1–20, doi:10.1080/01490419.2013.779334.

Holmes, S. A., and W. E. Featherstone (2002), A unified approach to the Clenshaw summation and the recursive computation of very high degree and order normalized associated Legendre functions, *J. Geod.*, *76*(5), 279–299, doi:10.1007/s00190-002-0216-2.
Holmes, S. A., and N. K. Pavlis (2008), Spherical harmonic synthesis software harmonic_synth. [Available at http://earth-info.nga.mil/GandG/wgs84/gravitymod/egm2008/index.html.]
Kuhn, M. (2000), *Geoidbestimmung unter Verwendung verschiedener Dichtehypothesen*, PhD thesis, Deutsche Geodätische Kommission, C. Reihe, No. 520, 128pp, München, Germany.
Kuhn, M. (2003), Geoid determination with density hypotheses from isostatic models and geological information, *J. Geod.*, *77*(1-2), 50–65, doi:10.1007/s00190-002-0297-y.
Kuhn, M., and W. E. Featherstone (2003), On the construction of a synthetic Earth gravity model, in *Proceed 3rd Meeting of the Intern. Gravity and Geoid Commission*, edited by I. Tziavos, pp. 189–194, Editions Ziti.
Kuhn, M., and K. Seitz (2005), Comparison of Newton's integral in the space and frequency domains, in *A Window on the Future of Geodesy*, IAG Symposia, vol. 128, edited by F. Sanso, pp. 386–391.
Kuhn, M., W. E. Featherstone, and J. F. Kirby (2009), Complete spherical Bouguer gravity anomalies over Australia, *Australian J. Earth Sci.*, *56*, 213–223.
Mader, K. (1951), Das Newtonsche Raumpotential prismatischer Körper und seine Ableitungen bis zur dritten Ordnung, Österreichische Zeitschrift für Vermessungswesen, Sonderheft 11.
Makhloof, A. A. (2007), The Use of topographic-isostatic mass information in geodetic applications, Dissertation, Institut für Geodäsie und Geoinformation der Universität Bonn, D 98.
Moritz, H. (2000), Geodetic reference system 1980, *J. Geod.*, *74*(1), 128–162, doi:10.1007/s001900050278.
Mohr, P. J., B. N. Taylor, and D. B. Newell (2012), The 2010 CODATA recommended values of the fundamental physical constants (Dated: March 25, 2012). [Available from http://physics.nist.gov/constants.]
Nagy, D. (1966), The gravitational attraction of a right rectangular prism, *Geophysics*, *31*, 362–371.
Nagy, D., G. Papp, and J. Benedek (2000), The gravitational potential and its derivatives for the prism, *J. Geod. 74*(7), 552–560.
Nagy M., et al. (2002), Erratum, *J. Geod. 76*(8), 475.
Novák, P. (2010), Direct modelling of the gravitational field using harmonic series, *Acta Geodyn. Geomater.*, *7*(1), 35–47.
Novák, P., and R. Tenzer (2013), Gravitational gradients at satellite altitudes in global geophysical studies, *Surv. Geophys.*, *34*, 653–673, doi:10.1007/s10712-013-9243-1.
Pavlis, N. K., and R. H. Rapp (1990), The development of an isostatic gravitational model to degree 360 and its use in global gravity modelling, *Geophys. J. Int.*, *100*, 369–378.
Papp, G., and Z. T. Wang (1996), Truncation effects in using spherical harmonic expansions for forward local gravity field modelling, *Acta Geod. Geophys. Hung.*, *31*(1-2), 47–66.
Rapp, R. H. (1989), The decay of the spectrum of the gravitational potential and the topography of the Earth, *Geophys. J. Int.*, *99*, 449–455.
Rapp, R. H., and N. K. Pavlis (1990), The development and analysis of geopotential coefficient models to spherical harmonic degree 360, *J. Geophys. Res.*, *95*(B13), 21,885–21,911.
Rummel, R., R. H. Rapp, H. Sünkel, and C. C. Tscherning (1988), Comparisons of global topographic/isostatic models to the Earth's observed gravity field, report No 388, Dep. Geodetic Sci. Surv., Ohio State University, Columbus, Ohio.
Sünkel, H. (1985), An isostatic Earth model, report No 367, Dep. Geodetic Sci. Surv., Ohio State University, Columbus, Ohio.
Tenzer, R. (2005), Spectral domain of Newton's integral, *Boll Geod. Sci. Affini*, *2*, 61–73.
Tenzer, R., P. Novák, P. Vajda, V. Gladkikh, and Hamayun (2012), Spectral harmonic analysis and synthesis of Earth's crust gravity field, *Comput. Geosci.*, *16*, 193–207, doi:10.1007/s10596-011-9264-0.
Torge W. (2001), *Geodesy*, 3rd ed., de Gruyter, Berlin and New York.
Tsoulis, D. (2001), A comparison between the Airy/Heiskanen and the Pratt/Hayfordisostatic models for the computation of potential harmonic coefficients, *J. Geod.*, *74*(9), 637–643, doi:10.1007/s001900000124.
Tsoulis, D., P. Novák, and M. Kadlec (2009), Evaluation of precise terrain effects using high-resolution digital elevation, models, *J. Geophys. Res.*, *114*, B02404, doi:10.1029/2008JB005639.
Tziavos, I. N., and M. G. Sideris (2013), Topographic reductions in gravity and geoid modeling, in *Lecture Notes in Earth System Sciences*, vol. 110, pp. 337–400, Springer, Berlin Heidelberg.
Wang, Y. M., S. Holmes, J. Saleh, X. P. Li and D. Roman (2010), A comparison of topographic effect by Newton's integral and high degree spherical harmonic expansion—Preliminary results, poster presented at WPGM 2010 Taipei, Taiwan, 22 –25 June.
Wang, Y. M., and X. Yang (2013), On the spherical and spheroidal harmonic expansion of the gravitational potential of topographic masses, *J. Geod.*, *87*(10-12), 909–921, doi:10.1007/s00190-013-0654-z.
Wieczorek, M. A. (2007), Gravity and topography of the terrestrial planets, in *Treatise on Geophysics, 10*, pp. 165–206, Elsevier-Pergamon, Oxford, U. K.
Wieczorek, M. A., and R. J. Phillips (1998), Potential anomalies on the sphere: Applications to the thickness of the lunar crust, *J. Geophys. Res.*, *103*(E1), 1715–1724, doi:10.1029/97JE03136.
Wild-Pfeiffer F., and B. Heck (2007), Comparison of the modelling of topographic and isostatic masses in the space and the frequency domain for use in satellite gravity gradiometry, in *Gravity Field of the Earth*, Proceed. 1st International Symposium of the International Gravity Field Service, Istanbul, Turkey, Harita Dergisi, 312–317.